JCTC Journal of Chemical Theory and Computation

Article

pubs.acs.org/JCTC

Duschinsky, Herzberg–Teller, and Multiple Electronic Resonance Interferential Effects in Resonance Raman Spectra and Excitation Profiles. The Case of Pyrene

Francisco J. Avila Ferrer,[†,∥] Vincenzo Barone,[‡] Chiara Cappelli,[‡,§] and Fabrizio Santoro[†,*]

[†]Consiglio Nazionale delle Ricerche – CNR, Istituto di Chimica dei Composti Organo Metallici (ICCOM-CNR), UOS di Pisa, Area della Ricerca, Via G. Moruzzi 1, I-56124 Pisa, Italy

[‡]Scuola Normale Superiore di Pisa, Piazza dei Cavalieri 7, I-56126 Pisa, Italy

[§]Dipartimento di Chimica e Chimica Industriale dell'Università di Pisa, Via Risorgimento 35, I-56126 Pisa, Italy

[∥]Physical Chemistry, Faculty of Science, University of Málaga, Málaga 29071, Spain

Supporting Information

ABSTRACT: We show that a recently developed time-independent approach for the calculation of vibrational resonance Raman (vRR) spectra is able to describe Duschinsky and Herzberg–Teller (HT) effects acting on a single resonant state, together with interferential contributions arising from multiple electronic resonances, allowing us to investigate in detail how their interplay determines both the vRR spectra at selected wavelengths and the Raman excitation profiles. We apply this methodology to the study of the spectra of pyrene in acetonitrile, an ideal system since it exhibits three close-lying electronic transitions that are bright but also subjected to HT effects. To single out the different contributions to vRR line shapes we adopted two different adiabatic models for resonant-state potential energy surfaces, namely, Adiabatic Shift (only accounting from equilibrium geometry displacements) and Adiabatic Hessian (AH, including also the Duschinsky effects), and Franck–Condon (FC) or HT approximations for the transition dipole. We show that, on balance, FC+HT calculations within the AH model provide the best agreement with experiment. Moreover, our methodology permits to individuate bands in the experimental spectra due to the simultaneous contribution of more than one resonant state and to point out and analyze interferential effects between the FC and HT terms in each resonance Raman process, together with FC-HT and HT-HT interferences between different electronic states.

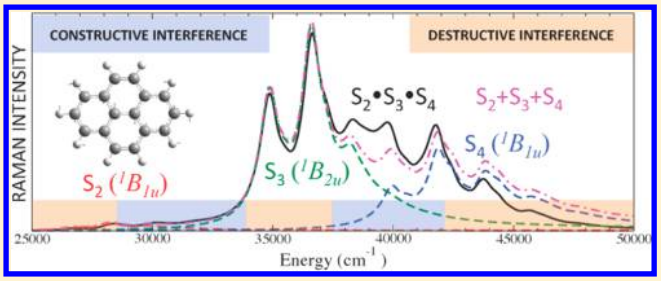

1. INTRODUCTION

Vibrational resonance Raman (vRR) spectroscopy[1−3] is a powerful technique to investigate the properties of excited states and the dynamical processes occurring on their potential energy surfaces (PES). This was clearly shown by Heller and collaborators[4,5] who derived a time dependent (TD) expression for the polarizability tensor in terms of time correlation functions determined by the dynamics of a wave packet promoted on the excited resonant state. TD expressions for one-photon absorption (OPA) spectra show an analogous correspondence on the time-evolution of the same wavepacket involved in vRR, although OPA is determined by its overlap with the initial vibrational state (as for Rayleigh elastic scattering) and vRR by overlap with a different vibrational state (the final state of the inelastic process).[4,5] A further difference between vRR and OPA spectra is that the excitation frequency ω_I is the frequency variable in OPA, whereas it is usually fixed in a vRR experiment where the variable is the so-called Raman shift, i.e., the difference between the fixed ω_I and the scattered frequency ω_S. While OPA and vRR in principle deliver similar information, vRR has the benefit of being intrinsically resolved on the vibrational modes; i.e., it provides information on the motion (for instance, the excited-state geometry displacement) along each mode. Such information is present also in the vibrational progressions of OPA spectra, but often it is not easily accessible, being blurred by multimode effects and, in polar solvents, by inhomogeneous broadening.[6]

Quantum Mechanical (QM) approaches have the potential to disentangle the role played by different molecular factors in determining spectroscopic signals.[7,8] Different approaches have been proposed for the computation of vRR spectra, such as the TD approach by Heller[4,5] and the Transform Theory (TT).[9] While these theories are in principle quite general, they must be approximated for dealing with sizable systems characterized by many (dozens/hundreds) normal modes and often, especially for large conjugated moieties, by a number of close-lying electronic states. For these systems, which are the focus of the present contribution, harmonic expansions of the initial and

Received: March 12, 2013
Published: June 17, 2013

   dx.doi.org/10.1021/ct400197y | J. Chem. Theory Comput. 2013, 9, 3597−3611

resonant state PES represent, at least, a necessary starting point for any evaluation of vibronic contributions.[7,10]

As an additional approximation on the PES, the most popular numerical implementations of vRR theories, within the TD approach [either adopting the so-called short-time-dynamics (STD) limit[4,5] or computing the true evolution of the wavepacket[11,12]], the TT theory,[9,13] or time-independent approaches[14] further assume that initial and resonant states share the same normal modes and frequencies. Therefore they only allow for the effect of equilibrium position displacements, neglecting frequency changes and Duschinsky effects[15] (in preresonance regime the STD approach is still valid even for anharmonic PES[4,5]). Even if in the recent years applications of these approaches have been very useful to simulate and interpret vRR spectra of many systems in gas phase and in solution[13,16−25] and they have been the base for the development of methods tailored for very large systems,[21] Duschinsky effects have been shown to give remarkable effects on absorption and circular dichroism one- and two-photon spectra[7,10,26−28] and in vRR, in the limited cases where they have been explored.[29−31]

The existence of close lying electronic states calls for the possibility of remarkable interstate couplings so that in principle a nonadiabatic model should be adopted. This has been done in some cases[32] but, despite the impressive progresses of methods like MCTDH,[33,34] quantum dynamical (QD) approaches still represent a very challenging task. Fortunately, while a nonadiabatic approach is mandatory when interstate couplings are so strong that vibronic eigenfunctions cannot be attributed anymore to a single electronic state, a number of effects due to the closeness of electronic states can be still described in a Born−Oppenheimer (BO) adiabatic framework, by general and effective protocols that can be straightforwardly applied to large systems. These include both the interferential effects in the polarizability tensor due to multiple electronic resonances, and the vibronic borrowing mechanisms. It can be shown from perturbation theory[6] that these latter effects can be included allowing for a linear dependence of the transition dipoles on the nuclear coordinates (HT, Herzberg−Teller effect) since, distorting nuclear structure, weakly absorbing states can slightly mix to strongly absorbing ones acquiring some OPA intensity.

Formal approaches for including Duschinsky and HT effects within TT theory and time-correlator formalism[35−38] were presented several years ago. More recently Huh and Berger[39] reviewed the potentialities of approaches based on the analytical evaluation of quantum time-correlation functions for the computation of several optical spectra, including vRR, and a practical time-dependent (TD) approach to account for Duschinsky and HT effects has been reported in literature.[31] Nonetheless, as a matter of fact, most of the vRR computations reported so far are based on models that neglect Duschinsky effects and only consider Franck−Condon (FC) transitions. Furthermore, they avoid the explicit calculation of the transition polarizability tensor as a function of the excitation energy, thus preventing the possibility to address multiple resonance effects.

On the basis of the methods we developed in the past for the calculation of steady-state absorption and emission electronic spectra,[7,40−45] in 2011 we presented an effective time-independent (TI) approach to include the effect of Duschinsky mixing and HT couplings in vRR calculations.[29] Here we show that such a protocol is also capable of including the effect of multiple electronic resonances, thus allowing a full analysis of the subtle interplay of PES characteristics (geometry displacements, frequency changes, and Duschinsky mixings), vibronic intensity borrowing (HT effects), and multiple resonances, on the vRR spectra. By accounting for all these possible contributions in a coherent way, our approach is also very well suited to analyze in detail the interferential effects that modulate vRR intensities.

It should be noticed that the methods proposed by Al-Saidi et al.[17] and by Jensen et al.[46] intrinsically include multiple resonance effects by computing the vRR from geometrical derivatives of the complex polarizability. Our approach, based on an explicit summation over the vibronic resonant states, allows disentangling the effect of each of them; as a drawback it can be time-consuming when the number of resonant states becomes large. Moreover the methods in refs 17 and 46 neglect Duschinsky effects between the initial and resonant state PES.

As a test case we investigate the vRR of pyrene in acetonitrile in the 333−225 nm range. Pyrene is an ideal system for our study because of the availability of a very rich set of experimental data reported in ref 47, the existence of three electronic exited states that fall in this energy range, the remarkable HT effects, and the high symmetry point D_{2h} group that strongly facilitates the analysis and the individuation of the factors (FC or HT, displacements, frequency-changes, Duschinsky, etc.) that modulate the vRR intensities. To the best of our knowledge this is the first example of a computational study able to address simultaneously Duschinsky, HT, and multiple electronic resonances effects on a sizable system taking into account all the vibrational degrees of freedom (72).

The paper is organized as follows: Section 2 briefly introduces the working expressions we adopted for the calculation of vRR spectra, Section 3 gives the computational details, and Section 4 reports our results, which are discussed in Section 5. Section 6 summarizes our main findings and reports some concluding remarks.

2. THEORY

The $\rho\sigma$th element ($\rho, \sigma = x, y, z$) of the polarizability tensor for a transition $|i\rangle \rightarrow |f\rangle$ due to a monochromatic incident (I) radiation with angular frequency ω_I impinging on the sample is

$$\alpha_{\rho\sigma}^{fi} = \frac{1}{\hbar}\sum_m \frac{\langle f|\mu_\rho|m\rangle\langle m|\mu_\sigma|i\rangle}{\omega_{mi} - \omega_I - i\gamma_m} + \frac{1}{\hbar}\sum_m \frac{\langle f|\mu_\rho|m\rangle\langle m|\mu_\sigma|i\rangle}{\omega_{mi} + \omega_I + i\gamma_m} \quad (1)$$

where μ_ρ is the ρ-Cartesian component of the electric dipole. The sum is taken over all possible intermediate states $|m\rangle$, $\hbar\omega_i$ and $\hbar\omega_m$ are the energies of states $|i\rangle$ and $|m\rangle$, respectively, $\omega_{mi} = \omega_m - \omega_i$ and, finally, γ_m is the lifetime of excited state $|m\rangle$. The second term in the right-hand side of eq 1 is off-resonant and becomes negligible when ω_I is close to resonance with the transition energy ω_{mi}, so that the transition probability is dominated by the first resonant term.

The directions of propagation of incident ($\mathbf{n}^I_0$) and scattered ($\mathbf{n}^S_0$) light (frequency ω_S) define the so-called scattering plane. The quantity of interest in usual Raman setups is the differential cross section with respect to the scattering solid angle Ω[2]

$$\sigma'(\omega_I, \omega_S) = \frac{\partial\sigma}{\partial\Omega} = \frac{I_S(\pi/2; \perp^S + \parallel^S, \perp^I)}{J} \quad (2)$$

where the scattered intensity I_S, with any polarization ($\perp^S + \|^S$) with respect to the scattering plane, is collected at $\theta = \cos^{-1}(\mathbf{n}^I{}_0 \cdot \mathbf{n}^S{}_0) = 90°$ and the incident field is polarized perpendicularly ($\perp^I$) and has an irradiance J. The expression for I_s is[2]

$$I_S\left(\frac{\pi}{2};\ \perp^S + \|^s,\ \perp^I\right) = \frac{{\omega_S}^4 J}{16{\varepsilon_0}^2 {C_0}^4 \pi^2}\frac{45a^2 + 7g^2 + 5d^2}{45} \tag{3}$$

where c_0 and ε_0 are the speed of light and the dielectric permittivity in a vacuum. The a, g, and d terms are functions of the molecular polarizability tensor and, therefore, are dependent on ω_I and ω_S, as well as on molecular parameters; they are the so-called "mean polarizability", "symmetric anisotropy", and "antisymmetric anisotropy" and are obtained by orientational average considering freely rotating molecules. They are[2]

$$a = \frac{\alpha^{fi}_{xx} + \alpha^{fi}_{yy} + \alpha^{fi}_{zz}}{3} \tag{4}$$

$$g^2 = \frac{1}{2}\left|\left|\alpha^{fi}_{xx} - \alpha^{fi}_{yy}\right|^2 + \left|\alpha^{fi}_{xx} - \alpha^{fi}_{zz}\right|^2 + \left|\alpha^{fi}_{yy} - \alpha^{fi}_{zz}\right|^2 + \frac{3}{2}\left(\left|\alpha^{fi}_{xy} + \alpha^{fi}_{yx}\right|^2 + \left|\alpha^{fi}_{xz} + \alpha^{fi}_{zx}\right|^2 + \left|\alpha^{fi}_{yz} + \alpha^{fi}_{zy}\right|^2\right)\right| \tag{5}$$

$$d^2 = \frac{3}{4}\left(\left|\alpha^{fi}_{xy} - \alpha^{fi}_{yx}\right|^2 + \left|\alpha^{fi}_{xz} - \alpha^{fi}_{zx}\right|^2 + \left|\alpha^{fi}_{yz} - \alpha^{fi}_{zy}\right|^2\right) \tag{6}$$

In the framework of the BO approximation we can write the vibronic states as a product

$$|e_k;\ v^k_l\rangle = |e_k\rangle \otimes |v^k_l\rangle \tag{7}$$

where $|e_k\rangle$ is the electronic state and $|v^k_l\rangle$ the associated vibrational state. In vRR the initial and final states belong to the ground electronic state $|e_g\rangle$ so that, by integrating over the electronic degrees of freedom, eq 1 reduces to

$$\alpha^{fi}_{\rho\alpha} = \frac{1}{\hbar}\sum_{k,m}\frac{\langle v^g_f|\mu^{gk}_\rho|v^k_m\rangle\langle v^k_m|\mu^{kg}_\sigma|v^g_i\rangle}{\omega_{km,gi} - \omega_I - i\gamma_k} \tag{8}$$

In eq 8 $\mu^{gk}_\beta = \langle e_g|\mu_\beta|e_k\rangle$, $\omega_{km,gi} = \omega_{e_k} + \omega_{v^k_m} - (\omega_{e_g} + \omega_{v^g_i})$, and the lifetimes γ_{km} of the intermediate states $|e_k;v^k_m\rangle$ are assumed to be independent from the vibrational state $|v^k_m\rangle$, so that it is possible to drop the m subscript out (γ_k). Notice that the summation is over both resonant electronic states (k) and their associated vibrational states (m). When the exciting frequency is in near resonance with the transitions to more than one excited electronic state $|e_k\rangle$, this can give rise to interferential features between their contributions. These effects can be taken into account computing the polarizability tensor $\alpha^{gk}_{\rho\sigma}$ for each resonant state $|e_k\rangle$, and then summing them before applying in eq 2.

Adopting harmonic approximation for the ground and resonant states PESs, vibrational states $|v^l_m\rangle$ of a given electronic state $|e_l\rangle$ are direct products of one-dimensional (1D) states $|m^l_j\rangle$ for each mode j, and $|v^l_m\rangle = |\mathbf{m}^l\rangle = |m^l_1\rangle \otimes |m^l_2\rangle \ldots |m^l_N\rangle$, with N being the number of normal coordinates and m^k_j the quantum number of mode j.

The sets of mass-weighted normal coordinates $\mathbf{Q}^g$ and $\mathbf{Q}^k$ of electronic states $|e^g\rangle$ and $|e^k\rangle$ are related through a linear transformation, first introduced by Duschinsky:[15]

$$\mathbf{Q}^g = \mathbf{J}\mathbf{Q}^k + \mathbf{K} \tag{9}$$

where $\mathbf{J}$ is the Duschinsky matrix and $\mathbf{K}$ is a column vector collecting the displacements between the equilibrium geometries of the two electronic PES.

The transition electric dipole μ^{gk} is in general an unknown function of the normal coordinates and is approximated by a Taylor expansion along $\mathbf{Q}^g$

$$\mu^{gk}_\rho = \mu^{gk}_\rho(0) + \sum_j \mu^{gk}_\rho(j)Q^g_j + \sum_{j,k}\mu^{gk}_\rho(j,k)Q^g_j Q^g_k \ldots \tag{10}$$

By restricting the expansion in eq 10 to the first order and substituting into eq 8, we get

$$\begin{aligned}\alpha^{fi}_{\rho\sigma} = {} & \frac{1}{\hbar}\sum_m \frac{\langle \mathbf{n}^{f,g}|\mu^{gk}_\rho(0)|\mathbf{m}^k\rangle\langle \mathbf{m}^k|\mu^{kg}_\sigma(0)|\mathbf{n}^{i,g}\rangle}{\omega_{km,gi} - \omega_I - i\gamma_k} \\ & + \frac{1}{\hbar}\sum_m \frac{\langle \mathbf{n}^{f,g}|\sum_l \mu^{gk}_\rho(l)Q^g_l|\mathbf{m}^k\rangle\langle \mathbf{m}^k|\mu^{kg}_\sigma(0)|\mathbf{n}^{i,g}\rangle}{\omega_{km,gi} - \omega_I - i\gamma_k} \\ & + \frac{1}{\hbar}\sum_m \frac{\langle \mathbf{n}^{f,g}|\mu^{gk}_\rho(0)|\mathbf{m}^k\rangle\langle \mathbf{m}^k|\sum_l \mu^{kg}_\sigma(j)Q^g_l|\mathbf{n}^{i,g}\rangle}{\omega_{km,gi} - \omega_I - i\gamma_k} \\ & + \frac{1}{\hbar}\sum_m \frac{\langle \mathbf{n}^{f,g}|\sum_l \mu^{gk}_\rho(l)Q^g_l|\mathbf{m}^k\rangle\langle \mathbf{m}^k|\sum_j \mu^{kg}_\sigma(j)Q^g_j|\mathbf{n}^{i,g}\rangle}{\omega_{km,gi} - \omega_I - i\gamma_k}\end{aligned} \tag{11}$$

The first term of eq 11 is the FC term, while the remaining terms arise from the dependence of the transition dipoles on the nuclear coordinates (HT terms). It should be noticed that eq 11 is not the full second−order expansion of the transition polarizability, since the latter would also include terms deriving from the quadratic dependence of one of the two transition dipoles. However, terms arising from the linear dependence of the transition dipoles are the most relevant to account for intensity-borrowing mechanisms in weak (or even dark) absorbing states. As a matter of fact, even considering all the quadratic terms, the last term on the right-hand side in eq 11 would be the only nonvanishing one for states that are completely dark at the FC level.

3. COMPUTATIONAL DETAILS

Ground state equilibrium geometry and Hessian have been computed at the DFT level, while for excited state energies we resorted to TD-DFT method. We adopted the PBE0 functional and the 6-31G(d) basis set. Acetonitrile (ACN) effects on the ground and excited states properties have been taken into account by the polarizable continuum model (PCM)[48] in the equilibrium regime. All electronic calculations have been performed with the Gaussian G09 package of programs.[49] Transition dipole derivatives have been computed by central differences at the excited-state equilibrium geometries (HT_f model, see ref 10; in the following the "f" subscript is dropped) as a side product of the numerical calculation of the excited-state Hessian. In this procedure, G09 internal routines identify the right electronic state after the geometrical displacement (10^{-3} Å) and ensure that its electronic wave function does not change sign. All three states of pyrene relevant for the present work exhibit a finite transition dipole. This allowed us to verify the correctness of the adopted strategy checking a posteriori that, at all the displaced geometries, the module of the transition dipole changes only slightly and its Cartesian

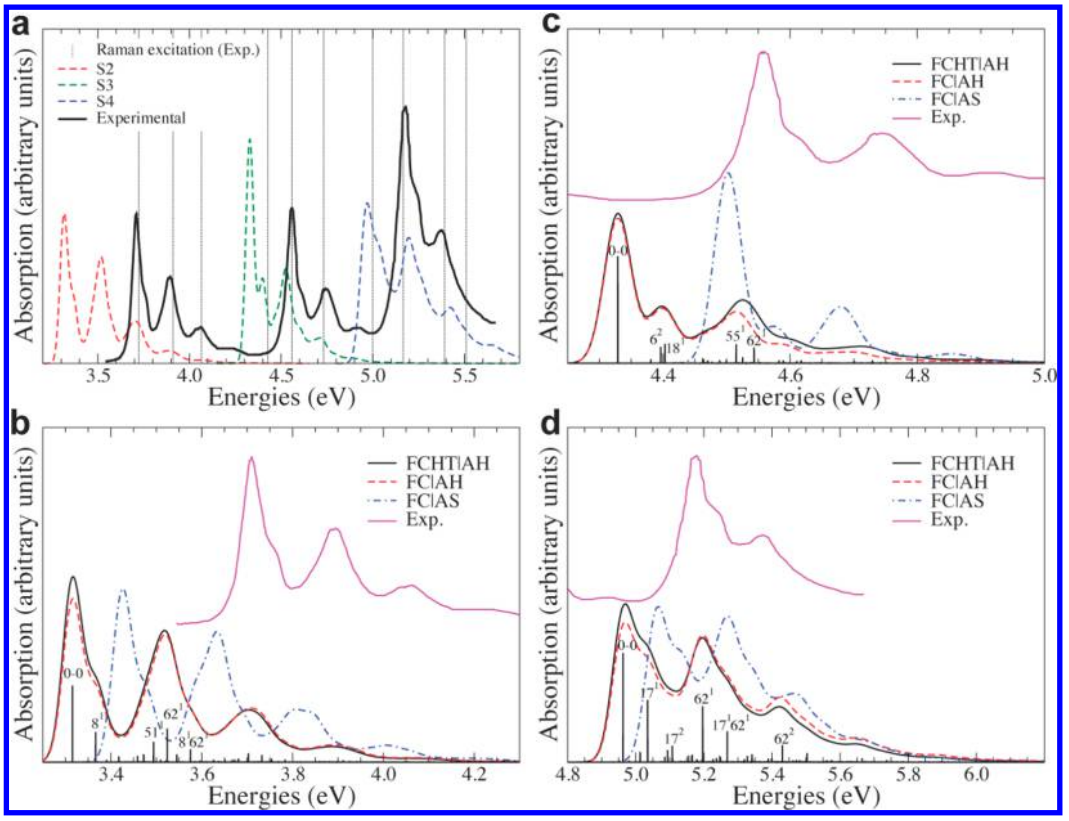

Figure 1. Panel (a) experimental (ref 47 black line) and computed (dashed lines) electronic absorption spectra of pyrene for the S_1, S_4, and S_8 electronic transitions in ACN with the FCHT|AH model. Panels (b), (c), and (d) compare the experimental spectra[47] (solid magenta lines), for S_1, S_4, and S_8, respectively, with those computed in ACN according to FCHT|AH (solid black), FC|AH (dashed red), and FC|AS (dashed blue) models. FCHT|AH stick spectra are also reported together with their assignments.

coordinate that is not null at the equilibrium geometry retains the same sign.

VRR spectra have been computed by a modified version of the **FC***classes* program[50] for fundamentals and overtones at 0 K. Recently, an effective method to compute vRR spectra at a finite temperature when Duschinsky and HT effects are negligible has been presented,[11] while for the general case when they have to be taken into account (i.e., our case) the calculation is still very challenging even if formal approaches have been proposed.[39] No remarkable temperature effect is expected in the vRR spectra of pyrene since, according to our calculations, all the ground state modes up to 400 cm^{-1} are nontotal symmetric and exhibit modest frequency changes and almost no Duschinsky mixing. In order to analyze the Duschinsky effects, two different models, Adiabatic Shift (AS) and Adiabatic Hessian (AH), have been adopted to describe the resonant state harmonic PES;[7,10,44] both approaches expand the PES around its own equilibrium geometry (adiabatic models), but differentiate in as much AS assumes the same normal modes and frequencies of the ground-state PES, while AH obtains them from the computation of the resonant state Hessian, thus including frequency changes and Duschinsky mixing effects. As far as the transition dipoles are concerned, both zero-order (FC) and first-order (FCHT) expansions in eq 10 are considered. In summary, the integrals entering in the expression of the polarizability tensor in eq 11 have been computed according to FC|AS, FC|AH, and FCHT|AH models. The vRR spectrum is obtained as a 2D function of the incident frequency ω_I and Raman shift $\omega_I - \omega_S$. Converged sums over the vibrational states associated to the resonant electronic state are obtained through an effective prescreening technique[29,40−43] that select the most important of them up to a maximum number (N^{max}). Convergence is checked by comparison between different calculation runs increasing N^{max} and with analytical sum for the elements of the transition polarizability tensor.[29] Multiple resonance effects are accounted for selecting, for each resonant state, the same set of final vibrational states and a common grid of points for ω_I and summing the corresponding polarizability tensors before computing the differential cross section in eq 2. All the vRR stick spectra and excitation profiles have been computed with a damping factor of 0.0544 eV while, for better visualization, the stick bands have been convoluted with a dimensionless Gaussian line shape with maximum equal to 1 and half width at half-maximum (HWHM) equal to 15 cm^{-1}.

4. RESULTS AND DISCUSSION

4.1. Electronic Absorption Spectra. The electronic excited states investigated experimentally in ref 47 and there labeled S_2 (B_{1u}), S_3 (B_{2u}), and S_4 (B_{1u}) correlate with computed S_1, S_4, and S_8 at the ground-state geometry and the PBE0/6-31G(d) level of theory [see Figure S1 in Supporting Information (SI) for a sketch of the involved molecular orbitals]. From now on they are identified as S_1, S_4, and S_8.

Figure 1 shows the computed absorption spectra for the S_1, S_4, and S_8 electronic transitions of pyrene at the FC|AS, FC|AH, and FCHT|AH level of theory and compares them with their experimental counterpart. In Figure 1a the vertical dotted black lines represent the excitation energies employed to measure vRR spectra.

dx.doi.org/10.1021/ct400197y | J. Chem. Theory Comput. 2013, 9, 3597−3611

The agreement with experiment is very good, both concerning the absolute position of the spectra and their band shape. For each state, both the spacing and relative intensity of the major progression and the existence of a secondary (lower-frequency) progression is correctly reproduced. The largest discrepancy is seen for the S_8 state, where the computed vibronic progression is significantly stronger than the experimental counterpart. This can be appreciated by looking at the relative intensity of the high-energy peaks with respect to the lowest energy (0−0) band, for each state. As expected, the AS model generally introduces an artificial blue-shift of the spectrum, due to the neglect of the difference of the normal modes and frequencies of ground and excited states.[7,10,26] The impact of these differences on the band shape is modest as witnessed by the similarity of AH and AS spectra; taking them into account slightly improves the agreement with experiment for S_4 and S_8 as far as the relative intensity of the vibronic peaks with respect to the 0−0 one is concerned. Introduction of HT effects modify only marginally the spectra lineshapes, slightly improving the relative intensity of the vibronic peaks.

Panels b−d of Figure 1 also report the main stick bands of the FCHT|AH spectra of S_1, S_4, and S_8 states, respectively, and their assignment n^x, where n is the normal mode and x its quantum number. As expected, the most intense transitions correspond to fundamentals, and those responsible for the observed different vibronic peaks involve collective stretchings of the fused rings coupled with in-plane C−H bendings; however, some combination bands, i.e., $8^1 62^1$ (S_1) and $17^1 62^1$ (S_8), have significant intensity, as well as some overtones of the b_{1u} low-frequency mode 6 (S_4) and of the collective stretching 62 (S_8). It is worthy to highlight that absorption bands are assigned in terms of excitations of excited-state normal modes and, due to differences in the Hessians in the AH model, in principle they are different with respect to the ground state and for each specific excited state. Table S1 in the Supporting Information associates the most-active excited-state modes in the absorption spectra with the most similar ones in the ground state (i.e., those showing the largest squared Duschinsky matrix elements). As it will be discussed in the following, in most cases, these latter are active in the vRR spectra and are sketched in Figure S2 in Supporting Information. Differences among the normal modes of the different states are striking for mode 6 (S_4), which projects on several S_0 modes (the largest projection being 0.38). The excited-state mode 62 for S_1 and S_8 practically coincides with the S_0 mode 62 (a_g symmetry), for S_4 it corresponds to the S_0 mode 59 (b_{3g} symmetry). This fact points out that the intense 62^1 band of the S_4 OPA spectrum is due to HT effects, in line with the very strong HT activity of the fundamental of the corresponding S_0 mode 59 in the vRR spectrum in resonance with S_4 (see below).

The computed spectra are slightly red-shifted with respect to experiment, by ∼0.4, 0.2, and 0.2 eV for S_1, S_4, and S_8, respectively. The relative intensity of the spectra of the three states nicely compares with experiment, apart from a slight overestimation of the S_4 extinction coefficient and an underestimation of the S_8 one. This latter is actually partially due to the overestimation of the vibrational progression that leads to a too broad (and hence less intense) spectrum. In summary, the spectral lineshapes for each state and their relative position and intensity, crucial parameters for multi-resonance effects, are nicely reproduced, supporting the reliability of our electronic data and the possibility to use them confidently to investigate the vRR spectra.

4.2. Vibrational Resonance Raman Spectra. A trivial source of error in the calculation of the vRR signal arises from inaccuracies in the computed transition energies, so that excitation frequencies that are in resonance with an electronic state in experiment can be off-resonant in simulations (or vice versa). Such an error does not only affect the absolute intensities, strongly dependent on the enhancement due to resonance, but also the relative intensities of a vRR spectrum. As an example, overtones and combination band intensities are expected to decay faster than fundamentals[12] and in general each vRR band has a different Raman excitation profile (see Section 4.3).

Vibronic and multiple electronic resonance effects on vRR are the focus of the present contribution and they can be better investigated eliminating (or at least strongly reducing) the effects of this source of error by determining excitation frequencies for the computation (ω_I^{com}) that exhibit resonance conditions roughly equivalent to those of the experimental ones (ω_I^{exp}) . In the present case, given the nice agreement between experimental and theoretical electronic absorption spectra, this can be done with good accuracy individuating for each ω_I^{exp} the experimental (ω_{00}^{exp}) and computed (ω_{00}^{com}) 0−0 transition frequency of the resonant state and determining ω_I^{com} with the following formula $\omega_I^{com} = \omega_I^{exp} - \omega_{00}^{exp} - \omega_{00}^{com}$.

Table 1 gives the modes most active in the computed vRR spectra (labeled in order of increasing frequency) and correlates them with observed bands, when such assignment is considered reliable. Theoretical bands are labeled as n^x where x indicates the number of quanta (if different from 0) on mode n in the final vibrational state. Computed frequencies generally overestimate experimental ones, as expected (see Table 1).[51] Such a

Table 1. Computed and Experimental Active Fundamentals of Pyrene in ACN

computed			experimental[a]
ω, cm^{-1}	mode	symmetry	ω, cm^{-1}
1712	62	a_g	1632
1667	59	b_{3g}	1597
1629	58	a_g	1553
1467	52	a_g	1408
1456	51	b_{3g}	(?)[b]
1440	50	b_{3g}	(?)[b]
1290	47	a_g	1242
1273	45	b_{3g}	(?)[b]
1176	40	a_g	1145[c]
1135	39	b_{3g}	1179[c]
1107	37	a_g	1067
604	17	a_g	592
505	12	b_{3g}	(?)[b]
462	9	b_{3g}	(?)[b]
412	8	a_g	408

[a]From ref 47. [b]It has not been possible to univocally determine the experimental counterpart. [c]Due to quasi-degeneracy, it is difficult to assign these two bands to modes 40 and 39 or vice versa. Our assignment is based on the observation that computed fundamental of mode 40 and the experimental band at 1145 cm^{-1} are active for spectra in resonance with the S_1 state, while the computed fundamental of mode 39 and the experimental band at 1179 cm^{-1} are not.

dx.doi.org/10.1021/ct400197y | J. Chem. Theory Comput. 2013, 9, 3597−3611

discrepancy is partly due to the combination of functional/basis set and partially due to the harmonic approximation.[52] The role of both factors can be evaluated by looking at the Table S1 in Supporting Information. The use of the B2LYP double-hybrid functional[52,53] in combination to a larger basis set substantially improves the predictions, which are further ameliorated by introducing anharmonic corrections (the latter calculated at the lower PBE0/6-31G(d) level, by following a protocol assessed by some of us[54]). In any case, the accuracy of PBE0/6-31G(d) harmonic frequencies is comparable with the other approximations involved in our general model, and for this reason, we will not apply corrections to such frequencies in the calculations of vRR spectra.

4.2.1. Single-State Resonance Raman Spectra. Figures 2−4 compare the experimental vRR spectra of pyrene at different excitation wavelengths and the computed vRR spectra for the S_1, S_4, and S_8 at equivalent excitation energies. Relevant vibrational modes are sketched in Figures S2 and S3 in Supporting Information. To avoid showing too many figures, the experimental spectra are given as insets; however, to highlight the correlations among the experimental and the theoretical peaks, we selected one representative excitation wavelength for each electronic state and, in Figure S4 of Supporting Information, we redraw the spectra connecting the corresponding bands with colored banners. It is worthy to notice that the explored wavelength region is off-resonant as far as ACN is concerned (λ_{max} = 195 nm), so that the excitation profile of solvent bands can be assumed to be rather flat. Therefore, although the experimental data are given in arbitrary units, the existence of a strong ACN band at 916 cm^{-1} (C═C stretching, ref 55) represents an internal standard that allows to individuate remarkable variation of the intensity of the pyrene bands with the excitation wavelength.

The computed vRR spectrum for the S_1 state is in nice agreement with experiment. The main bands at ∼400, ∼800, ∼1300, ∼1450, and 1700 cm^{-1} are all nicely reproduced and assigned to transition 8^1, 8^2, 47^1, 52^1, and 62^1, as well as a secondary band at 600 cm^{-1} (17^1), a minor peak on the red of the 1300 cm^{-1} peak (40^1), and a doublet on the red side of the band at 1700 cm^{-1} (58^1 and 59^1). Let us focus on the vRR spectrum for the lowest excitation energy (upper panel): the theoretical model correctly discriminates between intense and weak peaks, but the relative intensity of the major peaks show some discrepancy with experiment, such as, for example, the overestimation of the peak at 1632 cm^{-1} (experimental value). However, it is noteworthy that the relative changes of the vRR spectrum increasing ω_I^{exp} are nicely caught by our simulation, in fact: (i) the 62^1 band steeply increases with respect to the 47^1 and 52^1 one at 3.52 eV (middle panel) and then decreases again at 3.67 eV, and (ii) the low energy band at 400 cm^{-1} (8^1) decreases with respect to 62^1 at the increase of ω_I^{exp}. Inclusion of Duschinsky and HT effects has minor impact on the spectrum. It is noteworthy, however, that HT effect introduces an additional band 59^1 on the red wing of the one at 1712 cm^{-1} (computed value) and in that region the experimental spectrum does not show a single peak but rather a multiplet.

The analysis of the vRR spectrum in resonance with state S_4, given in Figure 3, deserves some special comment and is therefore postponed. Figure 4 shows that also the simulation of the vRR spectrum of the S_8 state is very satisfactory. As for S_1 all the main bands are correctly individuated and assigned to fundamental of modes 8, 17, 37, 39, 40, 52, 58, 59, and 62 from the red to the blue, respectively. Moreover, the simulation

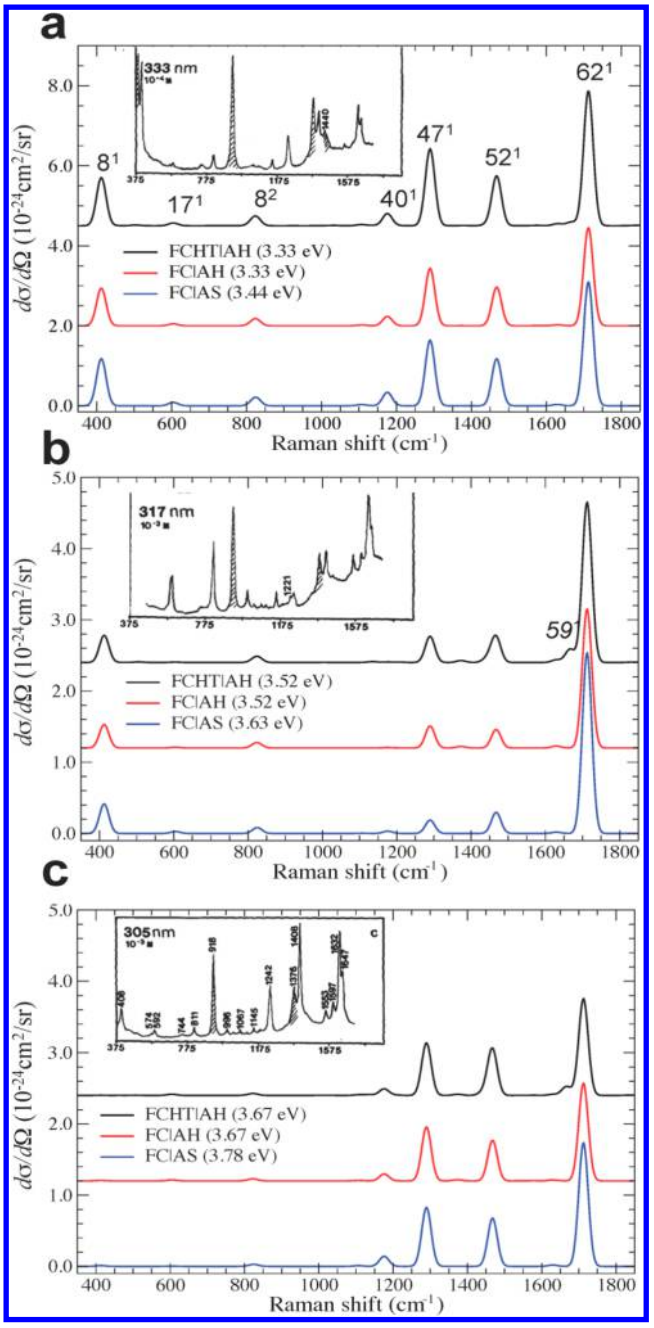

Figure 2. Experimental (insets, ref 47) and computed resonance Raman spectra at different excitation energies for the S_1 electronic excited state. Spectra were computed at FCHT|AH (black lines), FC|AH (red lines), and FC|AS (blue lines) levels. In the legend of each panel we report the theoretical excitation energy selected for each model in order to reproduce (see text) the resonance conditions taking place in the experiment at the following wavelengths: 333 nm (a), 317 nm (b), and 305 nm (c). Experimental spectra reprinted with permission from Jones and Asher, *J. Chem. Phys.* **1988**, *89*, 2649. Copyright 1988, American Institute of Physics.

catches very nicely the differences between the S_1 and S_8 state spectra. It is noteworthy the nice reproduction of the doublet at ∼1600−1700 cm^{-1} with the higher component that dominates the lower one and of the multiplet at 1100−1200 cm^{-1}, composed by an isolated band on the red edge (37^1) and a cluster of transitions at the blue edge, comprising fundamentals 39^1 and 40^1 and two overtones 17^2 and 16^2 modes. Very

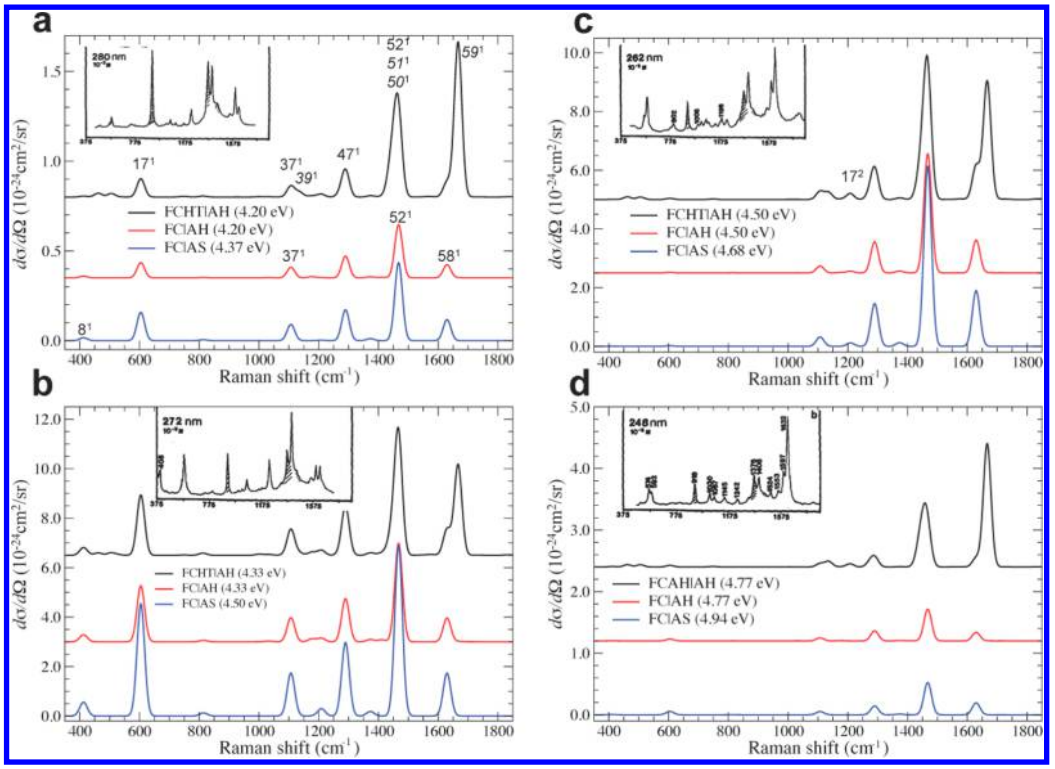

Figure 3. Experimental (insets, ref 47) and computed resonance Raman spectra at different excitation energies for the S_4 electronic excited state. Spectra were computed at FCHT|AH (black lines), FC|AH (red lines), and FC|AS (blue lines) levels. In the legend of each panel we report the theoretical excitation energy selected for each model, in order to reproduce (see text) the resonance conditions taking place in the experiment at the following wavelengths: 280 nm (a), 272 nm (b), 262 nm (c), and 248 nm (d). Experimental spectra reprinted with permission from Jones and Asher, *J. Chem. Phys.* **1988**, *89*, 2649. Copyright 1988, American Institute of Physics.

interestingly, the latter is due to a nontotal symmetric (b_{2g}), hence not-displaced mode (not active in the AS model), whose vRR activity arises from a large frequency change (146 cm^{-1}) in the $S_0 \rightarrow S_8$ transition. It is also remarkable that, in agreement with experiment, FCHT|AH predicts that with increasing ω_I^{exp} (middle and lower panels) a third weak band, assigned to the fundamental 59^1, grows between the two components of the doublet at 1600−1700 cm^{-1}. The dependence on ω_I^{exp} of the intensity of the multiplet at 1100−1200 cm^{-1} and of the low-frequency band at 600 cm^{-1} (decreasing from 240 to 230 nm and then increasing again up to 225 nm) is nicely reproduced too, even if the almost disappearance of band 17^1 (600 cm^{-1}) in the middle panel is in disagreement with experiment (230 nm). As discussed in Section 4.3, in proximity of such excitation wavelength, the Raman excitation profile of band 17^1 shows a point with vanishing intensity, but it rapidly increases both toward the red and the blue, so that the computed vRR intensity is strongly dependent on slight inaccuracies.

We now go back to the analysis of the vRR spectrum in resonance with state S_4. Figure 3 shows that the agreement is very satisfactory for Raman shifts <1500 cm^{-1}, i.e., excluding the high-energy multiplet. The major bands are correctly identified and assigned to fundamentals of modes 17, 37, 47, 52, 58, and 59. The 59^1 is a pure HT band, and in agreement with experiment, it is the most intense at 280 nm. It is noteworthy that our simulations nicely reproduce the dependence of the relative band intensities on ω_I^{exp}. This can be appreciated assuming that the intensity of the ACN band at 918 cm^{-1} is weakly dependent on ω_I^{exp} in the selected energy range. By comparison with this latter, we can deduce that the intensity of the pyrene band at 1440 cm^{-1} increases from 280 to 272 nm, stays constant until about 262 nm, and then decreases again at 248 nm. This is exactly what is predicted by our calculations. Moreover, it is interesting to notice that the pure HT bands 50^1, 51^1, and 59^1 dominate the spectrum in the preresonance (top-left panel) and postresonance (bottom-right panel) conditions. This can be appreciated by comparing FCHT|AH and FC|AH results and noticing that in the two spectra the peak at ∼1440 cm^{-1} falls at the same energy in the top-right and bottom-left panels (since it is dominated by the FC bands 52^1), while it is red-shifted at FCHT level in the other two panels (because the HT bands 50^1 and 51^1 become dominant). The same is true for the multipeak at ∼1650 cm^{-1} that, in the top-right and bottom-left panels, shows a red-shift shoulder (the FC 58^1 band) much more pronounced than in the other two panels (where the HT band 59^1 is by far more intense).

This analysis allows highlighting the main discrepancy with experiment. The blue component of the experimental doublet at ∼1600 cm^{-1} lies at 1632 cm^{-1}, and it was interpreted as the fundamental of a FC active a_g mode.[47] The agreement between simulated and computed spectra in resonance with the S_8 state (see Figure 4) allows us to assign it to the computed 62^1 band. Therefore, (i) the dominant 59^1 band of the computed spectrum in Figure 3 actually corresponds to the red component of the experimental doublet; (ii) the just perceivable experimental peak on the red side of the ∼1600 cm^{-1} doublet is assigned to the red shoulder in the computed spectrum (58^1), and (iii) the blue-component of the experimental doublet is completely missing in the simulated spectrum. Such band can be only reproduced abandoning the single-resonance approach adopted in this section and including in our model the possibility for quasi-resonances

dx.doi.org/10.1021/ct400197y | *J. Chem. Theory Comput.* 2013, 9, 3597−3611

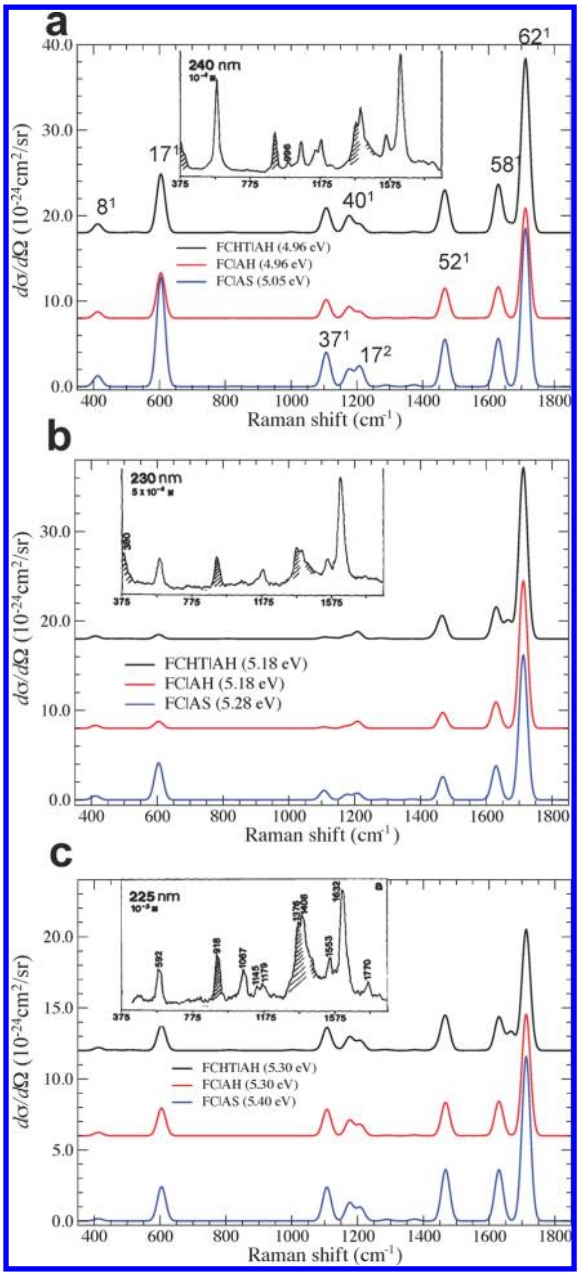

Figure 4. Experimental (insets, ref 47) and computed resonance Raman spectra at different excitation energies for the S_8 electronic excited state. Spectra were computed at FCHT|AH (black lines), FC|AH (red lines), and FC|AS (blue lines) levels. In the legend of each panel we report the theoretical excitation energy selected for each model, in order to reproduce (see text) the resonance conditions taking place in the experiment at the following wavelengths: 240 nm (a), 230 nm (b), and 225 nm (c). Experimental spectra reprinted with permission from Jones and Asher, *J. Chem. Phys.* **1988**, *89*, 2649. Copyright 1988, American Institute of Physics.

with more than one excited electronic state. Results are discussed in the next section.

4.2.2. Multistate Resonance Raman Spectra. The experimental multiplet at ~1600 cm^{-1} (in the excitation range 280–248 nm) is mainly a doublet whose blue component steeply increases with ω_I^{exp}. Data at 248 nm highlight also the existence of some secondary peaks on the red-edge of the band. Our calculations reported in Figure 3 cannot describe properly the structure of this band and the way it changes with ω_I^{exp}. Figure 5 shows that the results remarkably improve when we consider the simultaneous contribution of S_1, S_4, and S_8 states. In this way, in fact, the missing blue component of the multiplet appears, and its intensity increases with ω_I^{exp} in agreement with experiment, becoming comparable with the HT band 59^1 in the bottom-right panel (248 nm). Such a band is the 62^1 fundamental (1712 cm^{-1} according to calculations), and its intensity mainly derives from the preresonant contribution of state S_8.

The relative height of the 62^1 band is partially underestimated in our calculations, and it is predicted to appear at excitation frequencies larger than what are actually observed in experiment. These two facts are probably mutually correlated and both connected to the underestimation of the extinction coefficient of the S_8 band, as well as to the overestimation of the width of its spectrum. Additionally, in the following (Figure 6) we show that the 62^1 band is affected by HT effects arising from the coupling with the S_4 state (see below) so that it is reasonable that a simple perturbative treatment of the intensity borrowing (HT effect) cannot be fully adequate and that the intensity of this band is actually modulated by nonadiabatic couplings that would require a more accurate but very challenging variational treatment.

Comparison of FC|AS, FC|AH, and FCHT|AH results show that HT (mostly) and Duschinsky effects remarkably affect the vRR spectrum. While HT effect is able to introduce new bands unpredicted at the FC level, accounting for the differences in normal modes and frequencies of ground and excited state mainly introduces a modulation of some band intensity leading to their enhancement or de-enhancement (compare AH and AS results). This happens, for example, for the fundamental 62^1 for S_1 (see Figure 2), several transitions for state S_4 (Figure 3), and fundamentals 17^1 (600 cm^{-1}), 37^1 (1100 cm^{-1}), and 62^1 (1700 cm^{-1}) for state S_8.

4.3. Raman Excitation Profiles of the More Active Total Symmetric Fundamentals of the S_8 Transition. Computed vRR excitation profiles of the fundamentals of five FC active a_g modes for the S_8 electronic transition are plotted in Figure 6. The comparison of the profiles computed with the FC|AS and FC|AH models documents the existence of Duschinsky effects in the RR spectra of this system, while differences between FC|AH and FCHT|AH models put into evidence the presence and nature of HT contributions; these are not simply additive with respect to the FC terms but can give rise to interferential phenomena (see eq 11).

The similarity of computed and experimental Raman profiles confirms the nice agreement already observed at selected excitation energies for vRR spectra (notice that, in the insets of Figure 6, experimental data are given by the scattered points while continuous and dashed lines were obtained in ref 47 by fitting theoretical expressions of the Raman profiles to experimental data). All the investigated profiles can be essentially described like two or three multipeaked bands. It is remarkable that for transitions 17^1 (592 cm^{-1} in experiment) and 37^1 (1067 cm^{-1} in experiment) our results correctly predict that, between the main peaks, the Raman profile becomes vanishingly small.

Focusing on the long-wavelength multipeaked band, it can be noticed that inclusion of HT effects enhance/de-enhance its red/blue component, systematically improving the comparison with experiment (in agreement with the conclusions obtained in ref 47). Such an improvement is also evident looking at the relative height of the shorter wavelength bands with respect to

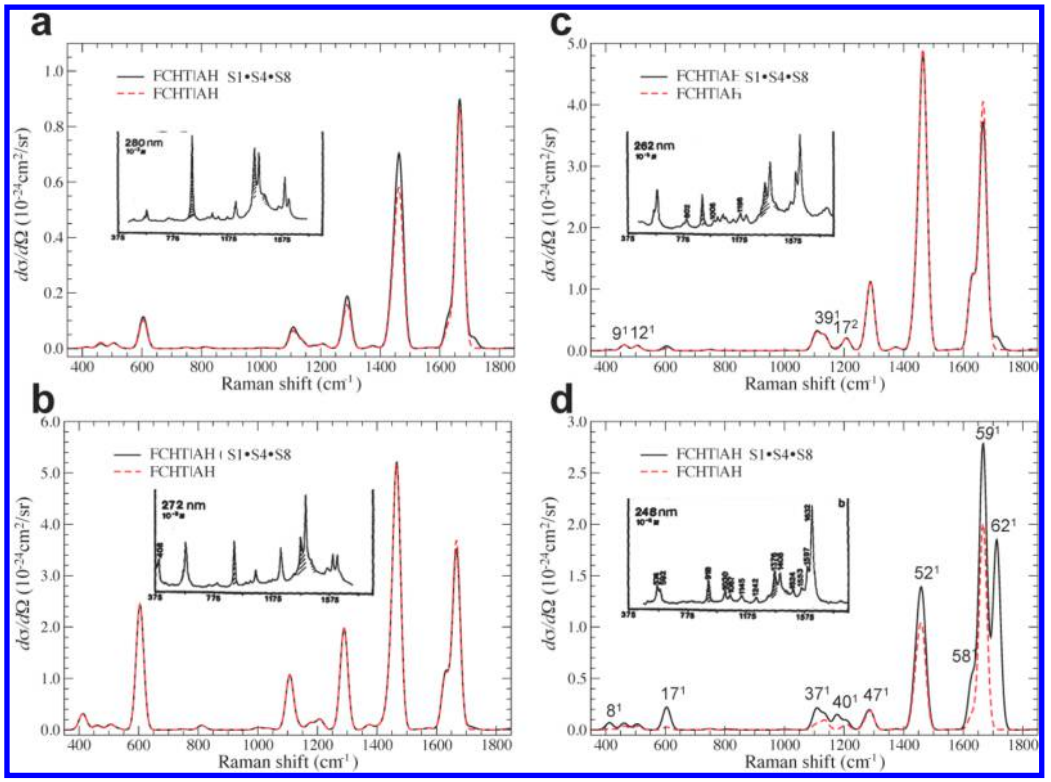

Figure 5. Experimental (insets, ref 47) and computed FCHT|AH resonance Raman spectra (black lines) at different excitation energies for the S_4 electronic excited state including the contribution of S_1, S_4, and S_8 electronic transitions in the polarizability tensor (S_1·S_4·S_8). Red dashed lines represent vRR spectra computed taking into account only the S_4 contribution: 280 nm (a), 272 nm (b), 262 nm (c), and 248 nm (d). Experimental spectra reprinted with permission from Jones and Asher, *J. Chem. Phys.* **1988**, *89*, 2649. Copyright 1988, American Institute of Physics.

the longest wavelength one. As it happens for absorption spectra,[10,26] comparison between AH and AS profiles show that neglecting the differences between ground state and excited state Hessians leads to a blueshift of the profile and a modulation of its band shape; AS profiles compare slightly worse with experiment. It is remarkable that, systematically, introduction of HT effects enhance/de-enhance the long-/short-wavelength portion of the Raman profile; de-enhancement in fact highlights interferences between the FC and HT contributions. An analogous effect, even if much weaker, is seen comparing FC|AH and FCHT|AH Raman profiles resonant with S_4 state (results not shown).

For a more detailed analysis, we focus for example on the fundamental 58^1 (at 1553 cm^{-1} in experiment). It is interesting to notice that even if its HT contribution to the absorption intensity is larger in S_4 than in S_8 (by this we mean that its contribution to the FCHT intensity,[10,42] relative to the FC intensity, is larger for S_4 (10%) than for S_8 (2%)) the HT effect on its Raman excitation profile is larger for S_8 than for S_4 (this latter profile is shown in Figure S4 in Supporting Information). This finding indicates that the HT effect on a Raman excitation profile of a fundamental of a given mode is a multimode effect, i.e., it depends on the HT effect along all the modes (the same happens for the absorption spectrum). Moreover, such an effect is not merely proportional to what happens in the absorption spectrum. As an example, while the HT effect enhances the blue wing of the S_4 absorption spectrum and de-enhances the blue wing of the S_8 one, it always de-enhances the blue-wing part of the Raman excitation profile of the vRR 58^1 band.

In the previous section we highlighted some discrepancy in the computed/experimental dependence of the intensity of selected bands on the excitation wavelength. Let us consider bands 17^1 and 37^1. According to our FCHT computations reported in the middle panel of Figure 4 they both practically vanish, at an excitation wavelength corresponding to 230 nm in experiment; on the contrary, in the experiment only the latter vanishes while the former is still detectable. The analysis of the Raman excitation profiles allows a better understanding of the origin of the observed discrepancy. The computed excitation wavelength with resonance conditions equivalent to 230 nm in experiment is 240 nm (ω_I^{com} = 5.18 eV, see Figure 4) for the AH model and 234 nm (ω_I^{com} = 5.28 eV) for the AS model. The computed AH profiles are almost vanishing at 240 nm for both 17^1 and 37^1 bands, in agreement with the very weak signals reported in middle panel of Figure 4. Their shapes are very similar to what was observed in experiment (see insets of Figure 6) where however the zero intensity is at 230 nm for the 37^1 band, but slightly shifted at ~232 nm for 17^1; this slight discrepancy explains why, for this latter band, some intensity is experimentally observed at 230 nm. The AS model is apparently in better agreement with experiment simply because at ω_I^{com} = 5.28 eV the profile is not vanishingly small, but considering the whole experimental Raman profile it is easy to recognize that actually the AH model and, most of all, FCHT|AH calculations provide the best agreement with experiment.

4.4. Interference between S_1, S_4, and S_8 Resonances. In this section we investigate the occurrence of interference between the contributions of different quasi-resonant electronic states in the excitation profiles of selected bands and the origin of this phenomenon. The top panels of Figure 7 show the Raman excitation profiles for two bands, i.e., 52^1 (panel a) and 59^1 (panel e), observed experimentally at 1408 cm^{-1} and 1597

dx.doi.org/10.1021/ct400197y | *J. Chem. Theory Comput.* 2013, 9, 3597−3611

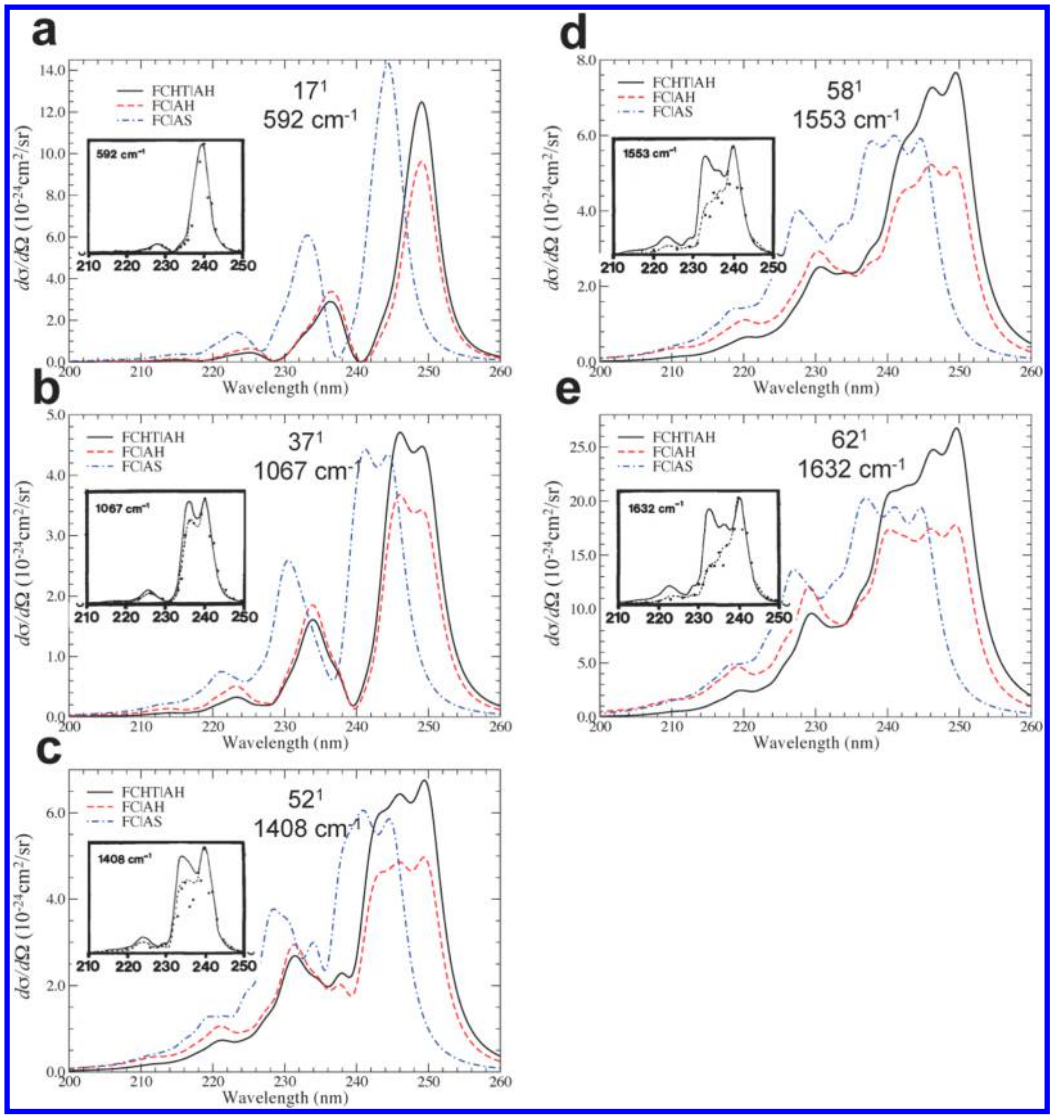

Figure 6. Resonance Raman excitation profiles for the a_g fundamentals of the S_8 transition of pyrene in ACN computed with FCHT|AH (black lines), FC|AH (dotted red lines), and FC|AS (dotted blue lines) models. Fundamentals 592 cm^{-1} (a); 1067 cm^{-1} (b); 1408 cm^{-1} (c); 1553 cm^{-1} (d); and 1632 cm^{-1} (e). The profiles computed in ref 47 and the experimental data (circles, ref 47) are reported as insets and are reprinted with permission from Jones and Asher, *J. Chem. Phys.* **1988**, *89*, 2649. Copyright 1988, American Institute of Physics.

cm^{-1} and computed respectively at 1434 cm^{-1} and 1667 cm^{-1} (1404 and 1589 cm^{-1}, respectively, at B2LYP including anharmonic corrections, see Supporting Information). The activity of band 59^1 is only due to HT effects, since this mode belongs to b_{3g} irreps, whereas band 52^1 is both FC and HT active. The excitation profiles obtained taking into account a single electronic state per time are compared with the excitation profiles obtained summing the contributions to the polarizability tensor of all the three states (we label this calculation as "$S_1{\cdot}S_4{\cdot}S_8$"). As we discussed in the method section, such a simultaneous contribution can give rise to interferential effects, and they are most conveniently highlighted by comparison with what was obtained by simply summing the single-state Raman profiles "$S_1{+}S_4{+}S_8$". Figure 7 clearly shows that, while the interferential effects are very modest for the band 52^1, they are remarkable for the pure HT band 59^1. Specifically, interference is strongly constructive at ∼5 eV, where the profiles of S_4 and S_8 are almost equally intense, increasing the intensity by ∼40%, while it is destructive in the red (in resonance with S_1) and blue (in resonance and post-resonance with S_8) wings of the profile.

The profiles of the fundamentals of other modes shown in Supporting Information indicate that what is observed in Figure 7 is a general trend and interferential effects are more effective on HT modes (compares Figure S5 and S6 in Supporting Information). Figure S5 in fact shows that interference has a small effect on the excitation profiles for totally symmetric (a_g) modes. Going in deeper detail, when HT effects are taken into account for a_g modes, the interference is destructive in the blue region of the S_4 electronic state and in the red region of the S_8 (left panels), but if we neglect the HT terms the interference effects disappear (right panels). A noticeable exception is band 52^1 (right panel c) that at FC level shows a weak constructive interference in the S_4 and S_8 overlap region, and a destructive one along S_4 and S_8 profiles.

With the aim of analyzing in further detail the interference mechanisms, Figure 7b–d (52^1) and Figure 7f–h (59^1) show the frequency dependence of the three invariants a^2, d^2, and g^2 (see eqs 4–6), whose sum according to eq 3 gives the vRR intensity, and Tables S3 and S4 in the Supporting Information give the contributions to the corresponding polarizability tensor

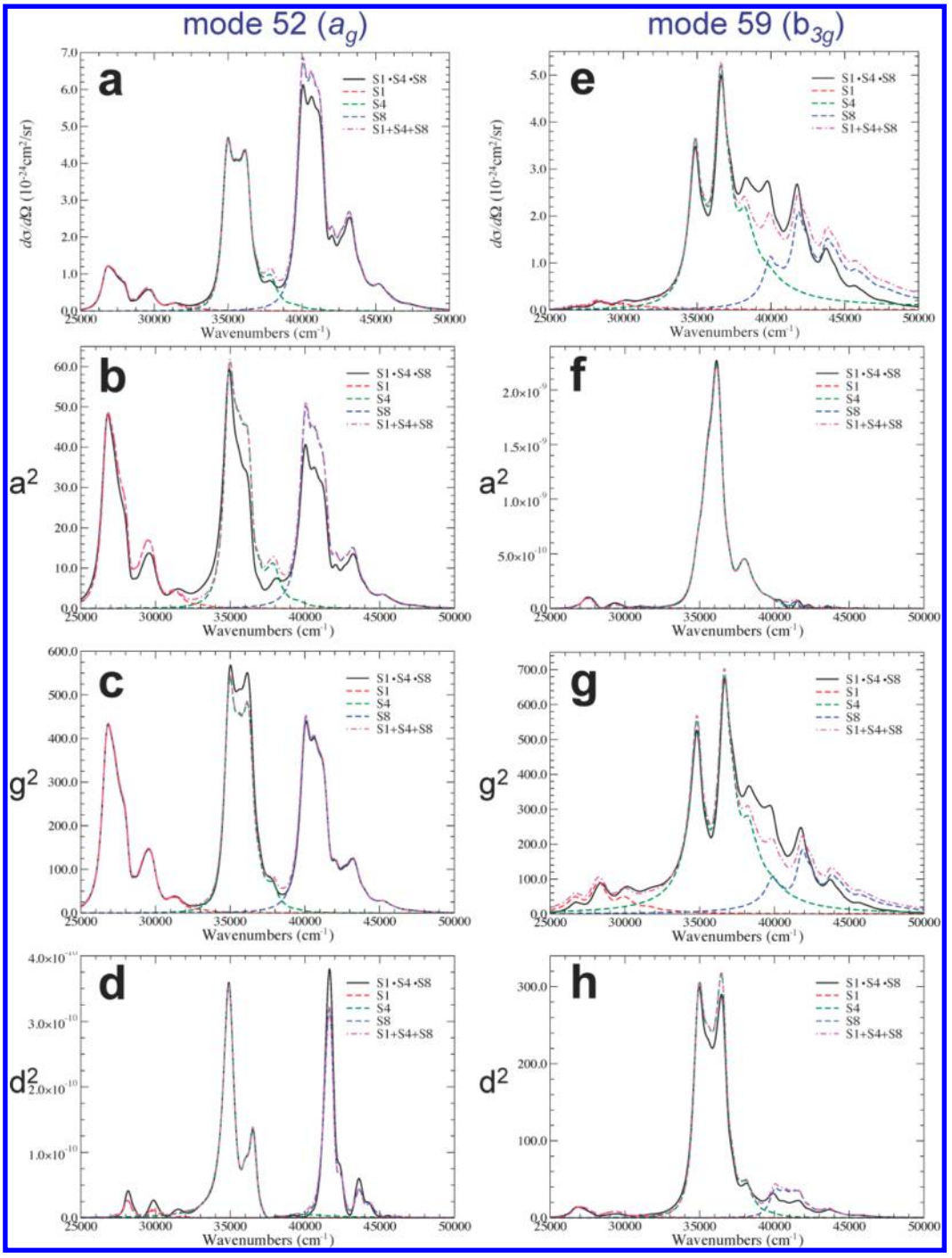

Figure 7. Raman excitation profiles of the 52^1 FC-active band (a) and the 59^1 HT-active band (b), in resonance with S_1 (red dashed line), S_4 (green dashed line), and S_8 (blue dashed line), sum of the latter three profiles (magenta dashed−dotted, S_1+S_4+S_8), and Raman profile obtained including the contributions of all the three states in the calculation of the polarizability tensor (black, S_1·S_4·S_8). Same analysis for the three invariants a^2, g^2, d^2 (see eqs 4−6) given in arbitrary units for the 52^1 band (panels b−d) and the 59^1 band (panels e−h).

α at the excitation frequencies ω_I^{com}, where interferential effects are maximal (respectively ω_I^{com} = 37300 cm^{-1} for 52^1 and ω_I^{com} = 39900 cm^{-1} for 59^1). It is useful to remember that the $S_0 \rightarrow S_1$ and $S_0 \rightarrow S_8$ transition dipoles are oriented along the z axis, while the $S_0 \rightarrow S_4$ transition is y-polarized. As expected, the 52^1 FC band takes most of its intensity from a^2 and g^2, while d^2 is practically vanishing (notice the scale in Figure 7d) because at FC level the α tensor is symmetric, but not exactly zero, because some minor HT effects do exist also for this FC-allowed band; on the contrary, the intensity of the 59^1 HT band mostly arises from the g^2 and d^2 components (HT contributions make α not symmetric) while the a^2 term, only arising from FC contributions, is vanishingly small. At ω_I^{com} 37300 cm^{-1} the interference is modest and destructive, while as mentioned above it becomes constructive, but vanishingly small, if we only consider FC terms. According to Table S3, S_1 and S_8 states show the expected strong α_{zz} component (due to the polarization of their transition with S_0), but a strong α_{zz} component also exists for S_4 and is due to the pure HT-HT contribution in the last term of the right-hand side of eq 11

dx.doi.org/10.1021/ct400197y | J. Chem. Theory Comput. 2013, 9, 3597−3611

(FC terms for S_4 only involve the *yy* component). The same mechanism gives also rise to weak α_{yy} components for S_1 and S_8 states. Most of the destructive effect arises from the algebraic sum of the FC α_{zz} components of S_1 and S_8 and the α_{zz} HT-HT contribution of S_4.

The interferential effect is much more remarkable for the HT band 59[1], and Figure 7 and Table S4 documents that it mainly takes place on g^2 invariant and mainly arises from the α_{yz} and α_{zy} components of S_4 and S_8, i.e., from mixed FC-HT contributions (second and third terms on the right-hand side of eq 11). This is in line with the fact that mode 59 (b_{3g}) mixes S_4 (B_{2u}) and S_8 (B_{1u}) states, so that, upon displacement along such a mode, S_4 and S_8 acquire respectively a *z*-polarized and *y*-polarized component of the transition dipole moment. The discussion up to now has highlighted that interference mostly comes from the fact that the polarizability tensors of different states share the same nonvanishing components (diagonal for 52[1], off-diagonal for 59[1]), and this is due in both cases to HT contributions.

A more detailed observation of Figure 7 indicates a second reason for the stronger interference on the HT band 59[1]: its Raman profiles associated to S_1, S_4, and S_8 states are broader than for band 52[1] and therefore show a stronger overlap. The origin of this phenomenon can be analyzed with a simple AS model comprising two modes Q_s and Q_u, with frequencies ω_s and ω_u, the former total-symmetric (*s*) and therefore FC-active and the latter nontotal symmetric (*u*) but HT-active. We consider, to fix the ideas, the resonant state S_4, say ω_{00} the transition frequency between the ground vibrational states, and denote the vibronic states as $|S_n; w_S^{(n)}, w_u^{(n)}\rangle$, where $w_S^{(n)}$ and $w_u^{(n)}$ are the quantum numbers along *s* and *u* modes in the state S_n. Assuming that the HT borrowing is due to a mixing with S_8, the $S_0 \rightarrow S_4$ FCHT transition dipole is $(0, \mu_{0y}, \dot{\mu}_z Q_u)$ $(|S_0\rangle\langle S_4| + |S_4\rangle\langle S_0|)$; moreover, we assume for simplicity that the displacement along *s* due to the $S_0 \rightarrow S_4$ transition is small, so that all the contributions $|S_0; w_S^{(0)}, w_u^{(0)}\rangle \rightarrow |S_4; w_S^{(4)} \pm m, w_u^{(4)}\rangle$ with $m \geq 2$ are negligible. Making reference to eq 11, the Raman transition $|S_0; 0_S^{(0)}, 0_u^{(0)}\rangle \rightarrow |S_0; 1_S^{(0)}, 0_u^{(0)}\rangle$ along the FC mode Q_s gains intensity from the following contributions (ω_I^{max} is the excitation frequency for which the contribution is maximal)

$$\alpha_{yy}: \mu_{0y}{}^2\langle 1_s^{(0)}|0_s^{(4)}\rangle\langle 0_s^{(4)}|0_s^{(0)}\rangle; \quad \omega_I^{max} = \omega_{00} \tag{12a}$$

$$\alpha_{yy}: \mu_{0y}{}^2\langle 1_s^{(0)}|1_s^{(4)}\rangle\langle 1_s^{(4)}|0_s^{(0)}\rangle; \quad \omega_I^{max} = \omega_{00} + \omega_s \tag{12b}$$

$$\alpha_{zz}: \frac{\dot{\mu}_z^2}{2\omega_u}\langle 1_s^{(0)}|1_s^{(4)}\rangle\langle 1_s^{(4)}|0_s^{(0)}\rangle; \quad \omega_I^{max} = \omega_{00} + \omega_u + \omega_s \tag{12c}$$

$$\alpha_{zz}: \frac{\dot{\mu}_z^2}{2\omega_u}\langle 1_s^{(0)}|0_s^{(4)}\rangle\langle 0_s^{(4)}|0_s^{(0)}\rangle; \quad \omega_I^{max} = \omega_{00} + \omega_u \tag{12d}$$

where we exploited the second quantization expression $Q_u = 1/(2\omega_u)^{1/2}(a_u + a_u^+)$ and the fact that in the AS model $\langle n_u^{(0)}|m_u^{(4)}\rangle = \delta_{nm}$ for the nontotalsymmetric mode Q_u. Notice that the last two HT-HT terms (arising from the fourth term on the right-hand side of eq 11) depend on $\mu_z{}^2$ and are much smaller than the first two FC-FC terms (first term in the right-hand side of eq 11) that are proportional to $\mu_{0y}{}^2$. More specifically, according to PBE0/6-31G(d) calculations $\mu_{0y}{}^2 = 5.8$ au, while the largest $\dot{\mu}_z{}^2/(2\omega_u) = 0.29$ (for mode 59). Considering that $\langle 1_s^{(0)}|1_s^{(4)}\rangle \approx \langle 0_s^{(0)}|0_s^{(4)}\rangle$, the two HT-HT terms are expected to be $\leq 1/20$ of the FC-FC ones. On the contrary, the $|S_0; 0_S^{(0)}, 0_u^{(0)}\rangle \rightarrow |S_0; 0_S^{(0)}, 1_u^{(0)}\rangle$ transition has the following mixed FC/HT (second and third terms in the right-hand side of eq 11) contributions

$$\alpha_{yz}: \mu_{0y}\dot{\mu}_z/\sqrt{2\omega_u}\,|\langle 0_s^{(0)}|0_s^{(4)}\rangle|^2; \quad \omega_I^{max} = \omega_{00} + \omega_u \tag{13a}$$

$$\alpha_{yz}: \mu_{0y}\dot{\mu}_z/\sqrt{2\omega_u}\,|\langle 0_s^{(0)}|1_s^{(4)}\rangle|^2; \quad \omega_I^{max} = \omega_{00} + \omega_u + \omega_s \tag{13b}$$

$$\alpha_{zy}: \mu_{0y}\dot{\mu}_z/\sqrt{2\omega_u}\,|\langle 0_s^{(0)}|0_s^{(4)}\rangle|^2; \quad \omega_I^{max} = \omega_{00} \tag{13c}$$

$$\alpha_{zy}: \mu_{0y}\dot{\mu}_z/\sqrt{2\omega_u}\,|\langle 0_s^{(0)}|1_s^{(4)}\rangle|^2; \quad \omega_I^{max} = \omega_{00} + \omega_s \tag{13d}$$

Their relative importance only depends on the ratio of the FC factors $|\langle 0_s^{(0)}|1_s^{(4)}\rangle|^2/|\langle 0_s^{(0)}|0_s^{(4)}\rangle|^2$. If the displacement along Q_s is not too small, these contributions to the vRR of the HT-active mode Q_u have more similar intensities than those that contribute to the vRR of the FC-mode Q_s, producing a broader Raman excitation profile. Moreover, removing the hypothesis of small displacements along Q_s, the FC-HT contributions to the vRR of Q_u become more numerous, while this happens only for the FC-FC contributions to the vRR of Q_s (the HT-HT contributions do not change), increasing the relative broadening of the Q_u-band Raman profile. In Figure 7, we actually take into account the effect of all the modes of pyrene, and each of them contributes to the vRR of 59[1] with terms like those in eqs 13a−13d. Moreover, the width of the S_4 OPA spectrum in Figure 1 indicates that the displacements along the total-symmetric modes are indeed not very small. These facts explain why the S_4 Raman profile of band 59[1] is broader than for band 52[1], and it can better overlap (and hence interfere) with the S_8 one.

As a last comment we notice that interference is extremely reduced for the FC band 62[1], even if it appears both in the S_8 region and in the S_4 region, due to preresonance with S_8; in fact, its vRR intensity only derives from nonoverlapping S_1 and S_8 contributions, whereas S_4, which lies between them, practically does not contribute (see Figure S7 in Supporting Information).

5. DISCUSSION

The vRR spectra of pyrene have been the subject of previous theoretical analysis by Jensen and Schatz[56] and by Neugebauer et al.[20] Both contributions considered a subset of the excitation wavelengths here investigated, namely, three different wavelengths 333, 272, and 240 nm, in resonance with S_1, S_4, and S_8 in ref 55 and a single wavelength 244 nm, in resonance with S_8 in ref 20. Moreover, in neither of the two papers were attempts made to simulate the full Raman excitation profiles, and overtones were not described. The calculations in ref 20 only accounted for FC transitions and did not take into account multiresonances and/or HT effects; these latter two factors were instead implicitly considered in the derivatives of the complex polarizability performed by Jensen and Schatz[56] and are very important to correctly describe the spectra in the S_4 region. Both the approaches in refs 20 and 56 are based on a STD approximation and therefore do not describe Duschinsky effects.

In general, our results qualitatively agree with those reported in refs 20 and 56 (see also ref 57). The computed frequencies in refs 20 and 56 are generally in better agreement with the

experimental values than our harmonic PBE0/6-31G(d) estimates. In this context, we showed in the Supporting Information that adoption of a double hybrid functional and inclusion of anharmonic corrections would provide frequencies extremely close to the observation. As far as the main focus of the present contribution is concerned, i.e., the relative intensities of the vRR bands, some improvements can be noticed in our predicted spectra with respect to the results in ref 56. In the vRR spectrum at 333 nm in resonance with S_1, our results correctly reproduce the overtone at ∼800 cm^{-1} (that cannot be described by the model in ref 56) and better describe the intensity of the band at ∼400 cm^{-1} that is strongly underestimated in ref 56. For the spectrum in resonance with the S_8 state at 240 nm, our results are closer to experiment as far as the relative intensity of band 58^1 (at 1553 cm^{-1} in experiment) and of the band 37^1 (at 1067 cm^{-1} in experiment) are concerned, since they are remarkably overestimated with respect to the dominant bands at 592 cm^{-1} and 1632 cm^{-1} in ref 56. Moreover, our calculations are able to better reproduce the relative intensity of the band at ∼1179 cm^{-1} (exp. value) with respect to the neighbor at 1067 cm^{-1}, and show that such a band is the result of different components, involving both fundamentals 39^1 and 40^1 and overtones 17^2 and 16^2. Similar improvements are seen with respect to the simulation of the spectrum at 244 nm presented in ref 20. Finally, considering the spectrum in resonance with the S_4 transition at 272 nm, our multiresonance calculations (see Figure 5) seem to describe slightly better the relative intensity of the bands lying in the experiment at 1067, 1242, 1408, and 1597 cm^{-1} (see most of all the bands at 1408 and 1067 cm^{-1}), while the agreement is worse for the 62^1 band (at 1632 cm^{-1} in experiment), whose intensity is much more underestimated in our calculations. As it is seen in Figure 5, in our calculations the contribution of this band correctly increases with the excitation frequency, but it is always underestimated with respect to experiment. The discrepancy probably arises from the underestimation of the ratio of the S_8 and S_4 oscillator strengths (2.1 with respect to the 3.2 value obtained in ref 56). It is however worthwhile to mention that our sum-overstates approach allows documenting that the appearance of such a 62^1 band is due to a preresonance contribution of the S_8 state, so that the underestimation of its intensity cannot be ascribed to a failure in the description of the displacement of S_4 PES along mode 62.

It must be stressed that a firm analysis of the origin of the discrepancies among our results and those given in refs 20 and 56 is not possible, because they can arise from differences in the DFT functional and basis adopted, in the medium (gas phase for refs 20 and 56, acetonitrile in our calculations) and in the methodology to compute vRR spectra. However, since most of the improvements seen in our calculations are obtained both at FClAH and FClAS level, we can deduce that that they are not due to the introduction of Duschinsky effects but, most probably, either to a better estimation of the differences of the ground- and excited-state PESs or to a more accurate account of vibronic effects, thanks to the evaluation of the transition polarizability through the explicit sum over the excited-state vibronic states.

6. CONCLUSIONS

In this contribution we presented a detailed analysis of the interplay of Duschinsky, Herzberg−Teller, and multiple electronic resonances on the vibrational Raman spectra and Raman excitation profiles of pyrene for excitation wavelength in resonance with its lowest three bright bands. We can summarize our main findings as follows:

(1) Herzberg−Teller Effects. vRR spectra are much more affected by HT effects than the absorption spectra. Specifically the HT mechanism gives rise to new bands (mainly in resonance with the S_4 state), observed in experiments but not predicted at the FC level. This is the case, for example, of one of the components of the multiplet at 1600−1700 cm^{-1} observed in vRR spectra in resonance with S_4 and S_8 states, that is due to the pure HT fundamental of mode 59 (1667 cm^{-1} in computations). Moreover introduction of HT effects remarkably improves the line shape of Raman excitation profiles.

(2) Duschinsky and Frequency-Changes Effects. They modulate both vRR spectra at selected excitations and the entire Raman excitation profiles. Unfortunately, the agreement of the computed and experimental spectra is only semi-quantitative and does not allow, in most of the cases, to check whether introduction of differences in the Hessians of ground and excited-state PESs leads to a real improvement of the results. Nonetheless our results show that such differences play a not-negligible role. In this situation, an apparent better agreement of AS models is due either to cancellation of errors or to an overestimation of Hessian differences by PBE0/6-31G(d) calculation. There are, however, some cases where their introduction clearly improves the agreement with the experiment. This happens, for example, for the Raman excitation profile of band 37^1, whose characteristic zero-intensity feature at 230 nm cannot be reproduced neglecting Hessian differences, and for the intensity of 16^2 overtone, since it is due to a change of the frequency of this mode on the S_0 and S_8 states that is not accounted for in AS models.

(3) Multiple Resonance Effects. For the vRR spectra with an excitation in the S_4 energy region, we show that it is necessary to take into account the contribution arising from preresonance with the S_8 electronic state. Otherwise, the 62^1 band is predicted to be inactive, while it is very strong in the experiment.

(4) Interferential Effects. Within a single-state approach we show that the interference between FC and HT contributions plays a relevant role in determining the experimental Raman excitation lineshapes. When considering the interferences arising from the quasi-resonance with more than one state, we document very strong effects in HT-active bands, and much more moderate effects on FC-allowed bands, pointing out that interference on a specific band may turn from positive to negative depending on the excitation wavelength. Our analysis shows that, both in the fundamental of FC-active and HT-active modes, interferential effects mainly arise from the linear dependence of the transition dipole on the normal modes (i.e., the HT effect).

In conclusion, to the best of our knowledge this contribution presents one of the most extensive first-principle computational analyses of pyrene vRR spectra. Besides the well-known interest of the specific system, on a general ground the results show that our TI sum-over-states methodology is effective enough to allow the simulation of full Raman excitation profiles for fundamentals, overtones, and combination bands,[29] including both Duschinsky and Herzberg−Teller effects, as well as the effect of multiple electronic resonances. Such efficiency is achieved thanks to a prescreening technique that is able to select only the vibrational states of the resonant state that contribute to the transition polarizability.[40−43]

The possibility to describe the full Raman excitation profile is particularly interesting in light of the results here presented, since they put into evidence that the strong dependence of the Raman profiles on the excitation wavelength and, most of all, the possible appearance of points where the vRR intensity is vanishingly small, can make the comparison of computed and experimental spectra at few selected wavelengths very sensible to slight inaccuracies and possibly induce misinterpretation. Computations of full Raman excitation profiles, on the other hand, allow a much more robust analysis and comparison with experiment.

■ ASSOCIATED CONTENT

Supporting Information

A table comparing harmonic and anharmonic frequencies; sketch of the molecular orbitals involved in the S_1, S_4, and S_8 transitions and the S_0 modes most active in vRR spectra. Analysis of interferential effects in the vRR of the fundamentals of several modes computed at FC and FCHT level. This material is available free of charge via the Internet at http://pubs.acs.org.

■ AUTHOR INFORMATION

Corresponding Author

*E-mail: fabrizio.santoro@iccom.cnr.it.

Notes

The authors declare no competing financial interest.

■ ACKNOWLEDGMENTS

The authors acknowledge the support of MIUR (FIRB "Futuro in Ricerca" RBFR10Y5VW and PRIN 2010-2011 2010ERFKXL), the Italian Institute of Technology (IIT-Seed HELYOS). F.J.A.F. acknowledges support from EU People Program, Marie Curie Actions (G.A. no. 246550).

■ REFERENCES

(1) Albrecht, A. C. *J. Chem. Phys.* **1961**, *34*, 1476−1484.
(2) Long, D. A. *The Raman Effect*; Wiley: Chichester, U.K., 2002; pp 221−266.
(3) Myers, A. B. *Chem. Rev.* **1996**, *96*, 911−926.
(4) Heller, E. J.; Lee, S.-Y. *J. Chem. Phys.* **1979**, *71*, 4777−4788.
(5) Heller, E. J.; Sundberg, R. L.; Tanor, D. *J. Phys. Chem.* **1982**, *86*, 1822−1833.
(6) Biczysko, M.; Bloino, J.; Santoro, F.; Barone, V. Time-independent Approaches to Simulate Electronic Spectra Lineshapes: From Small Molecules to Macrosystems. In *Computational Strategies for Spectroscopy: From Small Molecules to Nanosystems*; Barone, V., Ed.; John Wiley & Sons: Chichester, U.K., 2011; pp 361−446.
(7) *Computational Strategies for Spectroscopy*; Barone, V., Ed.; John Wiley & Sons: Hoboken, NJ, 2012; xi−xiii.
(8) Barone, V.; Baiardi, A.; Biczysko, M.; Bloino, J.; Cappelli, C.; Lipparini, F. *Phys. Chem. Chem. Phys.* **2012**, *14*, 12404−12422.
(9) Peticolas, L.; Rush, T. *J. Comput. Chem.* **1995**, *16*, 1261−1270.
(10) Avila, F.; Santoro, F. *Phys. Chem. Chem. Phys.* **2012**, *14*, 13549−13563.
(11) Petrenko, T.; Neese, F. *J. Chem. Phys.* **2012**, *137*, 234107−234119.
(12) Sun, Y.-P.; Miao, Q.; Mohammed, A.; Ågren, H.; Gel'mukhanov, F. *Chem. Phys. Lett.* **2011**, *511*, 16−21.
(13) Neugebauer, J.; Hess, B. A. *J. Chem. Phys.* **2004**, *120*, 11564−11577.
(14) Warshel, A.; Dauber, P. *J. Chem. Phys.* **1977**, *66*, 5477−5488.
(15) Duschinsky, F. *Acta Physicochim. URSS* **1937**, *7*, 551−566.
(16) Herrmann, C.; Neugebauer, J.; Presselt, M.; Uhlemann, U.; Schmitt, M.; Rau, S.; Popp, J.; Reiher, M. *J. Phys. Chem. B* **2007**, *111*, 6078−6087.
(17) Al-Saidi, W. A.; Asher, S. A.; Norman, P. *J. Phys. Chem. A* **2012**, *116*, 7862−7872.
(18) (a) Guthmuller, J.; Champagne, B. *J. Chem. Phys.* **2007**, *127*, 164507−164517. (b) Guthmuller, J.; Champagne, B. *J. Phys. Chem. A* **2008**, *112*, 3215−3223.
(19) Guthmuller, J.; Champagne, B.; Moucheron, C.; Kirsch De-Mesmaeker, A. *J. Phys. Chem. B* **2010**, *114*, 511−520.
(20) Neugebauer, J.; Baerends, E. J.; Efremov, E. V.; Ariese, F.; Gooijer, C. *J. Phys. Chem. A* **2005**, *109*, 2100−2106.
(21) Kiewisch, J.; Neugebauer, K.; Reiher, M. *J. Chem. Phys.* **2008**, *129*, 204103−204114.
(22) Luber, S.; Neugebauer, J.; Reiher, M. *J. Chem. Phys.* **2010**, *132*, 044113−044128.
(23) Mennucci, B.; Cappelli, C.; Cammi, R.; Tomasi, J. A. *Theor. Chem. Acc.* **2007**, *117*, 1029−1039.
(24) Mennucci, B.; Cappelli, C.; Guido, C. A.; Cammi, R.; Tomasi, J. *J. Phys. Chem. A* **2009**, *113*, 3009−3020.
(25) Kane, A. K.; Jensen, L. *J. Phys. Chem. C* **2010**, *114*, 5540−5546.
(26) Avila Ferrer, F. J.; Cerezo, J.; Stendardo, E.; Improta, R.; Santoro, F. *J. Chem. Theory Comput.* **2013**, *9*, 2072−2082.
(27) Lin, N.; Santoro, F.; Rizzo, A.; Luo, Y.; Zhao, X.; Barone, V. *J. Phys. Chem. A* **2009**, *113*, 4198−4207.
(28) Lin, N.; Solheim, H.; Ruud, K.; Nooijen, M.; Santoro, F.; Zhao, X.; Kwite, M.; Skowroneke, P. *Phys. Chem. Chem. Phys.* **2012**, *14*, 3669−3680.
(29) Santoro, F.; Cappelli, C.; Barone, V. *J. Chem. Theory Comput.* **2011**, *7*, 1824−1839.
(30) Priyutov, M. V.; Burova, T. G. *Opt. Spectrosc. (USSR)* **1991**, *71*, 37.
(31) Ma, H.; Liu, J.; Liang, W. Z. *J. Chem. Theory Comput.* **2012**, *8*, 4474−4482.
(32) Stock, G.; Woywod, C.; Domcke, W.; Swinneya, T.; Hudson, B. S. *J. Chem. Phys.* **1995**, *103*, 6851−6860.
(33) Beck, H.; Jäckle, A.; Worth, G. A.; Meyer, H.-D. *Phys. Rep.* **2000**, *324*, 1−105.
(34) *Multidimensional Quantum Dynamics. MCTDH Theory and Applications*; Meyer, H.-D., Gatti, F., Worth, G. A., Eds.; Wiley VCH: Weinheim, 2009; pp 1−7.
(35) Hizhnyakov, V.; Tehver, I. *J. Raman Spectrosc.* **1988**, *19*, 383−388.
(36) Chan, C. K.; Page, J. B. *J. Chem. Phys.* **1983**, *79*, 5234−5250.
(37) Tonks, D. L.; Page, J. B. *J. Chem. Phys.* **1988**, *88*, 738−760.
(38) Lu, H. M.; Page, J. B. *J. Chem. Phys.* **1990**, *90*, 5315−5326.
(39) Huh, J.; Berger, R. *J. Phys. Conf. Ser.* **2012**, *380*, 012019.
(40) Santoro, F.; Improta, R.; Lami, A.; Bloino, J.; Barone, V. *J. Chem. Phys.* **2007**, *126*, 084509−084521; **2007**, *126*, 169903.
(41) Santoro, F.; Lami, A.; Improta, R.; Barone, V. *J. Chem. Phys.* **2007**, *126*, 184102.
(42) Santoro, F.; Improta, R.; Lami, A.; Bloino, J.; Barone, V. *J. Chem. Phys.* **2008**, *128*, 224311.
(43) Santoro, F.; Barone, V. *Int. J. Quantum Chem.* **2009**, *110*, 476−486.
(44) Barone, V.; Bloino, J.; Biczysko, M.; Santoro, F. *J. Chem. Theory Comput.* **2009**, *5*, 540−554.
(45) Bloino, J.; Biczysko, M.; Santoro, F.; Barone, V. *J. Chem. Theory Comput.* **2010**, *6*, 1256−1274.
(46) Jensen, L.; Zhao, L. L.; Autschbach, J.; Schatz, G. C. *J. Chem. Phys.* **2005**, *123*, 174110−174120.
(47) Jones, C. M.; Asher, S. A. *J. Chem. Phys.* **1988**, *89*, 2649−2661.
(48) Tomasi, J.; Mennucci, B.; Cammi, R. *Chem. Rev.* **2005**, *105*, 2999−3094.
(49) Frisch, M. J.; Trucks, G. W.; Schlegel, H. B.; Scuseria, G. E.; Robb, M. A.; Cheeseman, J. R.; Scalmani, G.; Barone, V.; Mennucci, B.; Petersson, G. A.; Nakatsuji, H.; Caricato, M.; Li, X.; Hratchian, H. P.; Izmaylov, A. F.; Bloino, J.; Zheng, G.; Sonnenberg, J. L.; Hada, M.; Ehara, M.; Toyota, K.;Fukuda, R.; Hasegawa, J.; Ishida, M.; Nakajima,

T.; Honda, Y.; Kitao, O.; Nakai, H.; Vreven, T.; Montgomery, J. A., Jr.; Peralta, J. E.; Ogliaro, F.; Bearpark, M.; Heyd, J. J.; Brothers, E.; Kudin, K. N.; Staroverov, V. N.; Kobayashi, R.; Normand, J.; Raghavachari, K.; Rendell, A.; Burant, J. C.; Iyengar, S. S.; Tomasi, J.; Cossi, M.; Rega, N.; Millam, J. M.; Klene, M.; Knox, J. E.; Cross, J. B.; Bakken, V.; Adamo, C.; Jaramillo, J.; Gomperts, R.; Stratmann, R. E.; Yazyev, O.; Austin, A. J.; Cammi, R.; Pomelli, C.; Ochterski, J. W.; Martin, R. L.; Morokuma, K.; Zakrzewski, V. G.; Voth, G. A.; Salvador, P.; Dannenberg, J. J.; Dapprich, S.; Daniels, A. D.; Farkas, Ö.; Foresman, J. B.; Ortiz, J. V.; Cioslowski, J.; Fox, D. J. *Gaussian 09*, Revision A.2; Gaussian, Inc.: Wallingford, CT, 2009.

(50) Santoro, F. *FCclasses: A Fortran 77 Code*, 2008. Available via the Internet at http://village.pi.iccom.cnr.it; last accessed 24 May 2013.

(51) Barone, V. *J. Chem. Phys.* **2005**, *122*, 014108−014117.

(52) Biczysko, M.; Panek, P.; Scalmani, G.; Bloino, J.; Barone, V. *J. Chem. Theory Comput.* **2010**, *6*, 2115−2125.

(53) Grimme, S. *J. Chem. Phys.* **2006**, *124*, 034108−034123.

(54) Puzzarini, C.; Biczysko, M.; Barone, V. *J. Chem. Theory Comput.* **2010**, *6*, 828−838.

(55) Neelakantan, P. *Proc. Ind. Acad. Sci., Section A* **1964**, *60*, 422−424.

(56) Jensen, L.; Schatz, G. C. *J. Phys. Chem. A* **2006**, *110*, 5973−5977.

(57) The electronic character of the S_1, S_4, and S_8 states predicted at BP86/TZP level in ref 56 and at PBE0/6-31G(d) are very similar (compare Figure 8 in ref 56 with Figure S1 in Supporting Information) and the discrepancy in the irreps they belong to is only apparent and due to different conventions in the placement of the Cartesian axes; here we use the Mulliken convention.